WATER RESOURCES RESEARCH, VOL. 36, NO. 2, PAGES 411–420, FEBRUARY 2000

Groundwater waves in a coastal aquifer: A new governing equation including vertical effects and capillarity

L. Li and D. A. Barry

School of Civil and Environmental Engineering and Contaminated Land Assessment and Remediation Research Centre, University of Edinburgh, Edinburgh

F. Stagnitti

School of Ecology and Environment, Deakin University, Warrnambool, Victoria, Australia

J.-Y. Parlange

Department of Agriculture and Biological Engineering, Cornell University, Ithaca, New York

Abstract. Groundwater waves, that is, water table fluctuations, are a natural phenomenon in coastal aquifers. They represent an important part of the interaction between the ocean and aquifer and affect the mass exchange between them. This paper presents a new groundwater wave equation. Because it includes the effects of vertical flows and capillarity, the new equation is applicable to both intermediate-depth aquifers and high-frequency waves. Compared with the wave equation derived by *Nielsen et al.* [1997], the present equation provides a closer representation of groundwater waves. In particular, it predicts high-frequency water table fluctuations as observed in the field. A validation of the new equation has been carried out by comparing the analytical solutions to it with predictions from direct simulations using the numerical model SUTRA. The effects of various physical parameters and their relative importance are also discussed.

1. Introduction

A coastal aquifer is subject to dynamic boundary conditions at the ocean-land interface, which are characterized by the oscillations of the sea level (Figure 1). These oscillations are transmitted into the aquifer, the amplitude decreasing in the landward direction. Their influence, however, can be considerable up to a few hundred meters inland from the shore [*Lanyon et al.*, 1982]. The water table of the aquifer fluctuates in response to the sea level oscillations. These fluctuations are termed "groundwater waves." Below the water table the pressure within the aquifer also fluctuates. The groundwater fluctuations, as induced by the oceanic oscillations, affect water and mass exchange between the aquifer and ocean [*Li et al.*, 1999a].

Traditionally, groundwater waves are modeled using the Boussinesq equation. However, this equation is valid only for shallow aquifers where the assumption of negligible vertical flow holds. Recently, *Nielsen et al.* [1997] used analytical methods developed for surface waves to derive a governing equation for groundwater waves in aquifers of intermediate depths. A solution based on their governing equation was obtained for the water table fluctuations and the oscillating pressure field in a coastal aquifer:

$$h(x, z, t) = \mathrm{Re}\left[4a_0 \sum_{j=1}^{\infty} \frac{\sin(\kappa_j d)\cos(\kappa_j z)\exp(-\kappa_j x)\exp(i\omega t)}{2\kappa_j d + \sin(2\kappa_j d)}\right], \quad (1)$$

Paper number 1999WR900307.
0043-1397/00/1999WR900307$09.00

where x and z are the horizontal and vertical coordinates, respectively; t is time; h is the pressure fluctuation ($h(x, 0, t)$ gives the water table fluctuations); a_0 is the amplitude of the oceanic oscillation; κ is the wave number; j denotes wave mode; d is the thickness of the aquifer; $\omega = 2\pi/T$ is the frequency of the oscillations, where T is the period (Figure 1); Re denotes the real part of the function; and $i = \sqrt{-1}$. The solution is a summation of an infinite number of different wave modes. To obtain (1), a vertical ocean-land interface has been assumed with the following boundary condition applied at the interface [*Nielsen et al.*, 1997]:

$$h(0, z, t) = a_0 \cos(\omega t). \quad (2)$$

For each mode the following dispersion relation must be satisfied:

$$\kappa d \tan(\kappa d) = in\omega d/K, \quad (3)$$

where K and n are the hydraulic conductivity and porosity of the sand, respectively. Note that by setting $z = d$, one can obtain the solution for the water table fluctuations from (1). The wave number κ is a complex number; its real part represents the amplitude damping rate, and its imaginary part gives the phase shift. The behavior of the wave numbers is displayed in Figure 2. Only the first two modes are shown. As the frequency increases, the wave numbers quickly approach asymptotic values: $\pi/2d$ for the first mode and $3\pi/2d$ for the second mode. The general expression for the wave number asymptotes is

$$\kappa_j = \frac{(2j-1)\pi}{2d}. \quad (4)$$

The results shown in Figure 2 were obtained with variable ω and fixed values of n, K, and d. In general, the wave numbers

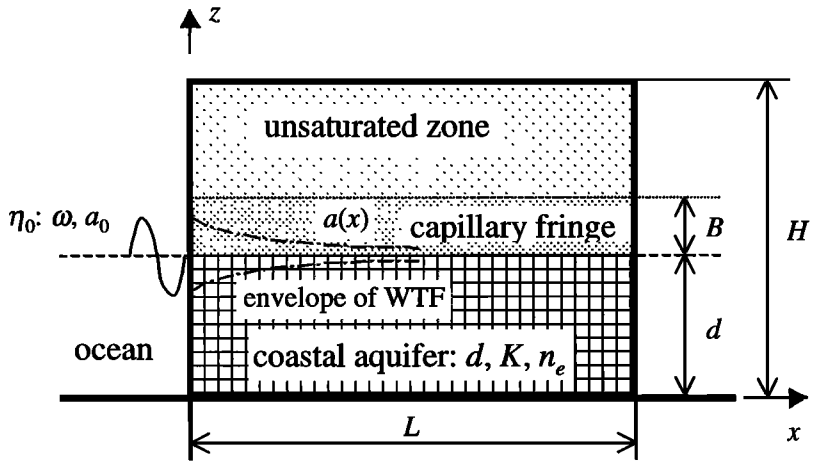

WTF: water table fluctuations

Figure 1. Schematic diagram of a coastal aquifer and the groundwater waves.

approach the asymptotes as $n\omega d/K$ (the nondimensional frequency) increases. With these asymptotic wave numbers the solution, (1), becomes nonanalytic at $z = d$. It predicts zero water table fluctuations with finite vertical velocities ($w = -K\partial h/\partial z$) at the free surface (except for $x = 0$, where w is undefined). Such behavior is obviously nonphysical as it violates the free-surface boundary condition and contradicts the field observations of high-frequency water table fluctuations [*Waddell*, 1976; *Lewandowski and Zeidler*, 1978; *Hegge and Masselink*, 1991; *Turner and Nielsen*, 1997; *Li et al.*, 1999b].

However, *Li et al.* [1997] investigated the influence of oceanic oscillations on coastal aquifers and determined two mechanisms of groundwater fluctuations. They found that capillary effects are important for high-frequency oscillations and provide the mechanism for high-frequency groundwater waves. A two-dimensional boundary-element model was developed to simulate the groundwater wave propagation in the aquifer. Capillary effects were incorporated into the model through the free-surface boundary condition using the approach of *Parlange and Brutsaert* [1984]. The inclusion of capillary effects enables the model to predict high-frequency water table fluctuations. In this paper we derive a new equation for groundwater waves by incorporating capillary effects into the intermediate-depth wave equation of *Nielsen et al.* [1997]. The new solution will be compared with previous solutions, and its validity will be checked against the results from direct simulations using SUTRA, a numerical model developed by *Voss* [1984].

The paper is organized as follows: First, the new equation with the capillary effects included is presented in section 2. Then, the differences between the present solution and previous ones are discussed. Next, validation of the new solution is carried out in section 3 using direct numerical simulations from SUTRA. Finally, conclusions are drawn in section 4.

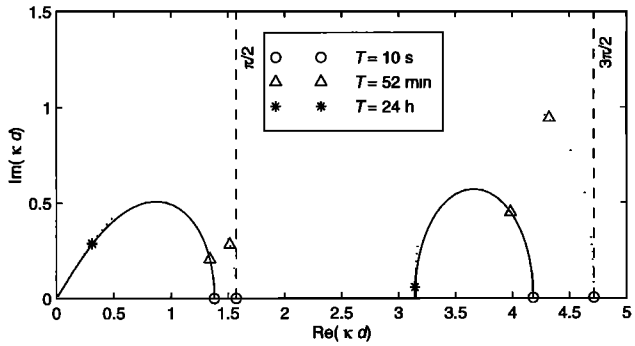

Figure 2. Variation of κ with frequency as predicted by *Nielsen et al.* [1997] (dotted curve) and the present equation (solid curve). In the calculation, $K = 0.00049$ m s^{-1}, $d = 3$ m, $n = 0.45$, and $B = 0.19$ m.

2. New Groundwater Wave Equations With Capillary Effects

Using a Rayleigh expansion of the potential function in terms of the aquifer depth, *Nielsen et al.* [1997] derived a groundwater wave equation, which includes the effects of vertical flows, that is,

$$\frac{\partial \eta}{\partial t} = \frac{K}{n} \tan\left(d\frac{\partial}{\partial x}\right)\frac{\partial \eta}{\partial x}, \tag{5}$$

where η is the fluctuation of the water table and $\tan[d(\partial/\partial x)]$ is an infinite order differential operator as defined by *Nielsen et al.* [1997]. Following *Parlange and Brutsaert* [1984] and *Li et al.* [1997], we derive a new groundwater wave equation from (5);

$$\frac{\partial \eta}{\partial t} = \frac{K}{n} \tan\left(d\frac{\partial}{\partial x}\right)\frac{\partial \eta}{\partial x} + \frac{B}{n}\frac{\partial}{\partial t}\left[\tan\left(d\frac{\partial}{\partial x}\right)\frac{\partial \eta}{\partial x}\right], \tag{6}$$

where B is the thickness of the capillary fringe (Figure 1). The details of the derivation are given by *Parlange and Brutsaert* [1984] and *Li et al.* [1997] and thus are omitted here. Essentially, the technique is based on the Green-Ampt approximation applied to the capillary fringe. The second term on the right-hand side of (6) accounts for capillary effects on ground-

water waves. An interpretation of this term's physical meaning is given in section 3.1. It should be noted that (6) is in linearized form, implying that only small-amplitude oscillations are considered here. *Nielsen et al.* [1997] also assumed this restriction in order to obtain analytical solutions.

2.1. Wave Dispersion

On the basis of (6) the dispersion relation is expressed as

$$\kappa d \tan(\kappa d) = \frac{in\omega d}{K + i\omega B}. \tag{7}$$

This new dispersion relation is different from that of *Nielsen et al.* [1997] as described by (3). The extra term in the denominator is due to the inclusion of the capillary term in (6). The solution for the oscillating pressure in the coastal aquifer subject to the oceanic oscillation as described by (2) is of the same form as (1); however, the dispersion relation that determines κ for each mode is now given by (7). As the oscillation frequency ω increases, the right-hand side of (7) approaches a finite number, nd/B, different from the behavior of (3). It can be shown that the free-surface boundary condition takes the following form:

$$n\frac{\partial \eta}{\partial t} = w(x, d, t) + \frac{B}{K}\frac{\partial}{\partial t}w(x, d, t). \tag{8}$$

Compared with the normal linearized free-surface boundary condition, (8) has an extra term on the right-hand side (i.e., the second term). This term accounts for the apparent water exchange between the aquifer and capillary fringe that occurs when the water table fluctuates [*Li et al.*, 1997].

In Figure 2 we show the new dispersion relation in comparison with that of *Nielsen et al.* [1997]. The following parameter values were used in the calculation: $K = 0.00049$ m s^{-1}, $d = 3$ m, $n = 0.45$, and $B = 0.19$ m. Significant differences between the two become evident as the frequency of the oscillation increases, showing the importance of capillarity for high-frequency oscillations. Moreover, as the frequency increases, the wave numbers now approach asymptotic values different from those given by (4). This is a fundamental difference between the present solution and that of *Nielsen et al.* [1997]. Recall that the latter becomes nonphysical at the free surface at the high-frequency limit; there are no water table fluctuation with finite vertical velocities. This situation does not arise in the present solution. As the frequency of the oscillation increases, capillarity starts to affect the process and changes the behavior of the wave number. At the high-frequency limit the wave number for each mode is less than that given by (4); the solution, (1), remains analytic at $z = d$ and predicts water table fluctuations.

2.2. Predicted Groundwater Waves (Comparison With *Nielsen et al.* [1997] and *Barry et al.* [1996])

In Figure 3 we show the high-frequency groundwater waves as predicted by the present analytical solution. The following parameter values were used in the calculation: $K = 0.00049$ m s^{-1}, $d = 3$ m, $n = 0.45$, $T = 10$ s, and $B = 0.19$ m. In contrast, *Nielsen et al.*'s [1997] solution predicts no water table movement. It is interesting to note that at high frequencies (i.e., $n\omega d/K \to \infty$), the water table fluctuations respond simultaneously to oceanic oscillations because the imaginary part of the wave number vanishes at high frequencies. In other words, the water table fluctuations become a standing wave.

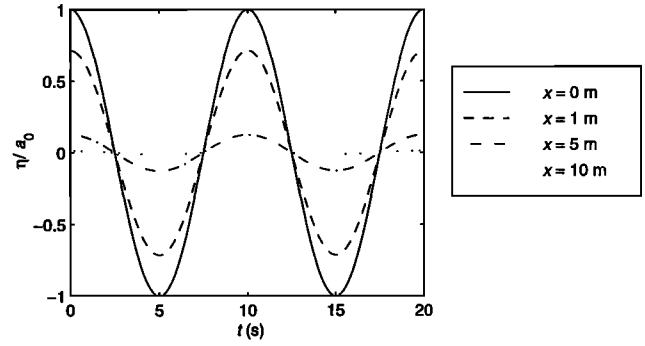

Figure 3. High-frequency water table fluctuations predicted by the present analytical solution. $K = 0.00049$ m s^{-1}, $d = 3$ m, $n = 0.45$, $B = 0.19$ m, and $T = 10$ s.

This feature has been observed in the field and is discussed by *Li et al.* [1997].

To examine the amplitude damping, we notice that at high frequencies, (1) can be rewritten as $h(x, d, t) = a_0 A(x) \exp(i\omega t)$. In Figure 4a we plot the normalized amplitude of the water table fluctuations against x. Assuming that $A(x)$ is of an exponential form, that is, $A(x) = \exp[-k(x)x]$, we fitted the simulation results on a curve and found that $k(x) = 4.4682 \times 10^{-4}x^4 - 1.2769 \times 10^{-2}x^3 + 1.3687 \times 10^{-1}x^2 - 6.8115 \times 10^{-1}x + 2.0307$. *Barry et al.* [1996] solved the modified Boussinesq equation with capillarity correction [*Parlange and Brutsaert*, 1984] for water table responses to boundary oscillations,

$$\eta = a_0 \exp(-k_1 x) \cos(\omega t - k_2 x), \tag{9a}$$

with

$$k_1 = \sqrt{\frac{n\omega}{2d}\left[\frac{1}{\sqrt{K^2 + (\omega B)^2}} + \frac{\omega B}{K^2 + (\omega B)^2}\right]}, \tag{9b}$$

$$k_2 = \sqrt{\frac{n\omega}{2d}\left[\frac{1}{\sqrt{K^2 + (\omega B)^2}} - \frac{\omega B}{K^2 + (\omega B)^2}\right]}. \tag{9c}$$

Note that this solution includes capillarity but no vertical flow effects. According to (9) the amplitude of water table decays inland exponentially, that is, $A(x) = \exp(-kx)$, where k is a constant. For the values of K, d, n, ω, and B used in the above calculation, k equals 0.8885. In contrast, the present solution predicts that k varies with x. The predicted amplitude damping in the near-shore region is greater than that given by (9) as shown in Figure 4b. The damping rate, however, decreases with the distance inland and becomes less than the constant rate (i.e., 0.8885) predicted by *Barry et al.* [1996]. In other words, tailing of water table fluctuations farther inland compensates the high-amplitude damping in the near-shore region. The difference between these two solutions is due to the effects of the vertical flow in the aquifer of an intermediate depth as observed in the field [*Nielsen*, 1990; *Kang et al.*, 1994]. In Figure 5 we show the amplitude damping observed in the field [*Kang et al.*, 1994] in comparison with the predictions of the analytical solution, (1). The agreement between the two is reasonably good, and both indicate a nonexponential amplitude damping. Mathematically, the nonexponential amplitude damping is caused by the presence of several modes of waves with different wave numbers. The vertical flow effects are reduced as the

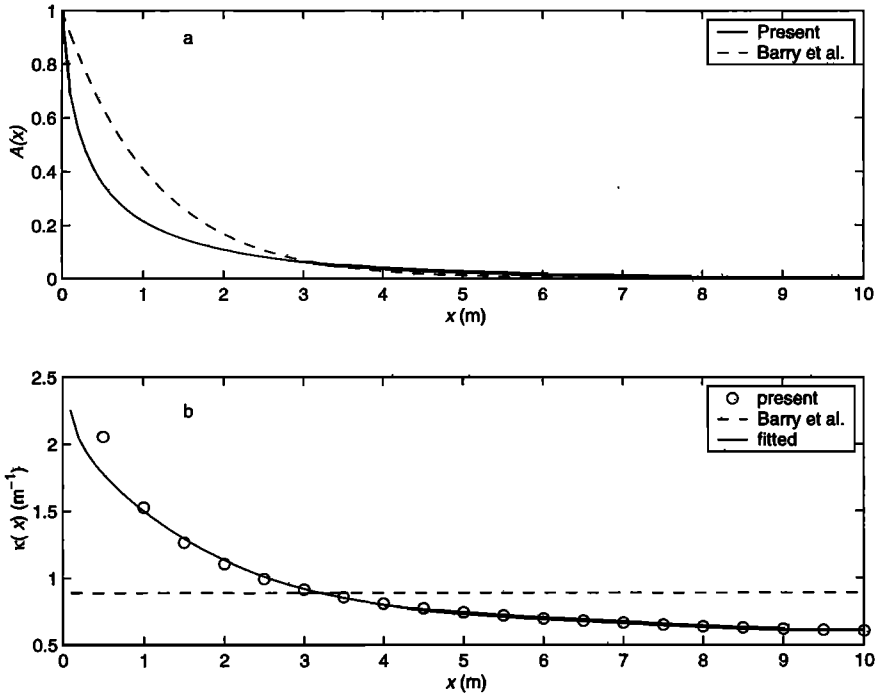

Figure 4. Comparison of the wave damping predicted by the present analytical solution and *Barry et al.* [1996]: (a) variations of normalized wave amplitude with the cross-shore distance and (b) wave-damping rate.

aquifer depth decreases. The influence of the aquifer depth on the groundwater waves will be discussed further in section 3.

According to the model of *Nielsen et al.* [1997], that is, (1) and (3), there exist no fluctuations of the water table at high frequencies, but the internal pressure oscillates, and the amplitude of the pressure fluctuations increases with the depth (i.e., $d - z$). In Figure 6 we compare the results of pressure fluctuations with the present solution and the results of *Nielsen et al.* [1997] based on the same parameter values as above. Large differences exist between the predictions of the two solutions. Near the shore (e.g., $x = 1$ m) the differences are larger close to the water table ($z = 3$ m) than in the deeper areas (z near 0), suggesting that the difference of pressure fluctuations (in the aquifer) is essentially caused by different water table behavior in both solutions. This trend, however, is reversed in areas farther inland (e.g., $x = 5$ m) because the pressure fluctuation at depth is influenced by not only the local water table fluctuations but also the seaward pressure field; the latter factor becomes more important with increasing depth and distance inland. As the distance from the shore increases, differences between the two solutions in deep areas become relatively large in relation to differences of the solutions near the water table. At both locations, less amplification of the pressure fluctuation with the depth is observed in the predictions of the present solution (Figures 6c and 6d). Note that in Figures 6c and 6d, the inverse of the amplification factor is plotted.

The difference between the predictions from the present solution and those of *Nielsen et al.* [1997] decreases as the wave period increases (i.e., $\omega B/K \rightarrow 0$) since capillary effects then become negligible [*Li et al.*, 1997].

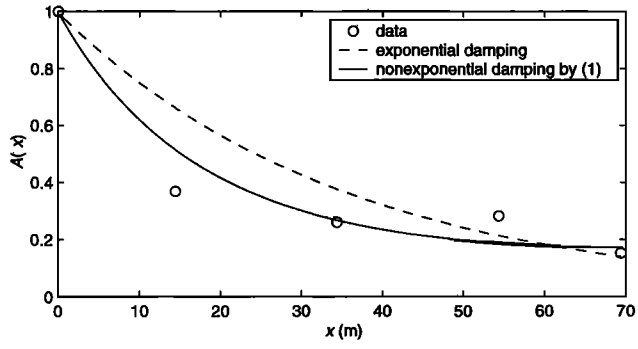

Figure 5. Comparison of the amplitude damping predicted by the present analytical solution and that observed in the field [*Kang et al.*, 1994].

3. Direct Simulation of Groundwater Waves Using SUTRA

To verify the present analytical solution, we carried out numerical simulations of the groundwater fluctuations using SUTRA, an existing finite element code [*Voss*, 1984]. This code models saturated/unsaturated groundwater flow and uses the three-parameter formula of *van Genuchten* [1980] for describing the relationship between the saturation and pressure in the unsaturated zone, that is,

$$s - s_{re} = \frac{1 - s_{re}}{[1 + (\alpha p)^{n_1}]^{n_2}}, \tag{10}$$

where s is the water saturation, s_{re} is the residual saturation, and p is the capillary pressure. Here α, n_1, and $n_2 = (n_1 - 1)/n_1$ are the three empirical parameters that determine the shape of the retention curve in the unsaturated zone. Two different types of retention characteristics were used in the simulations with $s_{re} = 0$, $\alpha = 0.00005$ Pa^{-1}, and $n_1 = 2$ and $s_{re} = 0$, $\alpha = 0.00005$ Pa^{-1}, and $n_1 = 4$, respectively. The retention curves are shown in Figure 7 where the water saturation is plotted against the vertical eleva-

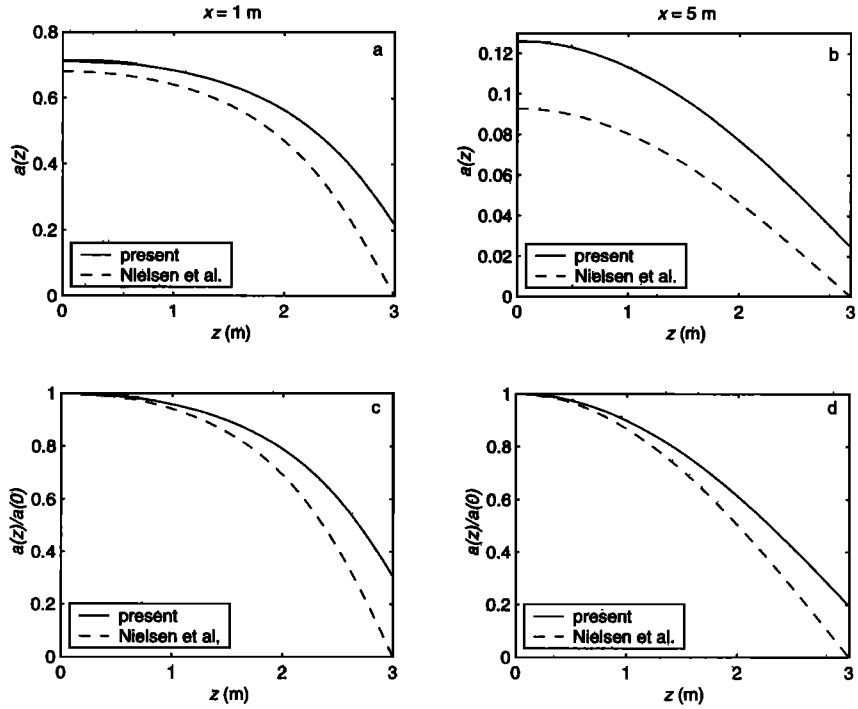

Figure 6. Comparison of the amplitude of the pressure oscillations predicted by the present analytical solution and *Nielsen et al.* [1997]: (left) (a and c) $x = 1$ m and (right) (b and d) $x = 5$ m. Here $a(z)$ is the amplitude of the pressure oscillations at z.

tion. The thickness of the capillary fringe is estimated as 0.19 m and 0.42 m for the first (Figure 7b) and second (Figure 7c) retention curves, respectively. The values of other model parameters for each simulation are listed in Table 1.

3.1. High-Frequency Groundwater Waves

The simulated high-frequency water table fluctuations from Sim1 are shown in Figure 8. These groundwater waves are similar to those displayed in Figure 3 as predicted by the

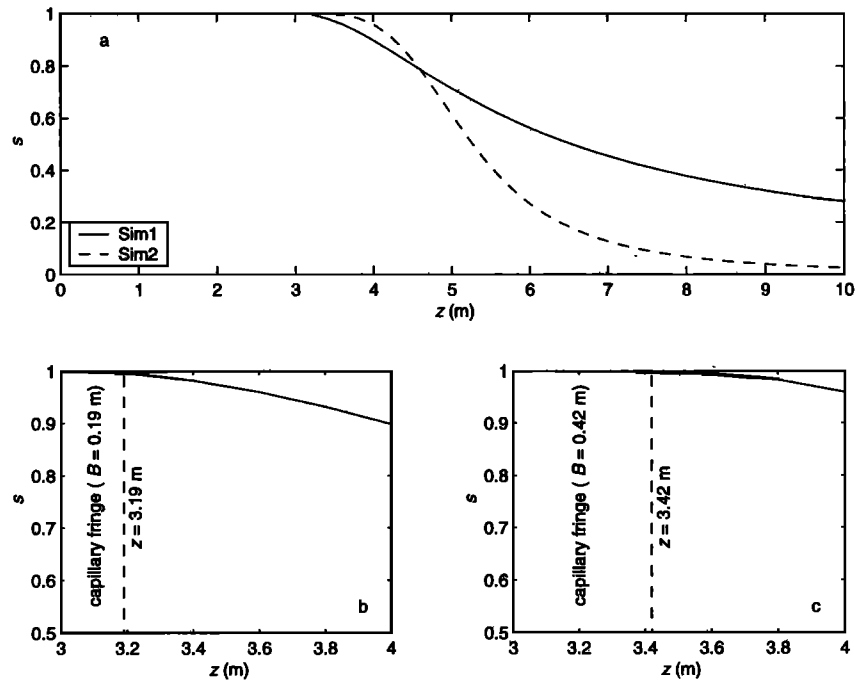

Figure 7. Water retention curves used in the simulations.

Table 1. Values of Model Parameter Used in the Simulations

	Model Parameters					
Simulation	d, m	K, m s^{-1}	T, s	a_0, m	B, m	Size of the Simulation Domain ($L \times H$), m^2
Sim1	3	0.00049	10	0.15	0.19 (first retention curve)	10 × 10
Sim2	3	0.00049	10	0.15	0.42 (second retention curve)	10 × 10
Sim3	0.1	0.00049	10	0.01	0.19	10 × 1
Sim4	70	0.00049	10	0.5	0.19	100 × 100

Here $n = 0.45$ for all simulations.

present wave equation; in particular, they are simultaneous groundwater responses to the oscillations at the boundary with the amplitude decreasing inland. Differences between the numerical and analytical results mainly exist in the falling phase. The numerical simulation showed that a seepage face was formed as the sea level fell. The seepage face dynamics are not included in the analytical solution. The vertical dotted-dashed curve in Figure 8 indicates that the peaks of the water table fluctuations occurred simultaneously at all locations.

To verify the analytical prediction of the wave damping, we calculated the normalized wave amplitude from the simulated water table fluctuations as $A(x) = a(x)/a_0$ and $a(x) = \eta_{max}$. The results are compared with those predicted by the present analytical solution with $B = 0.19$ m, as shown in Figure 9a. Also plotted in Figure 9 is the prediction from the boundary element model of *Li et al.* [1997]. This model simulates the two-dimensional saturated flow in the aquifer and includes capillary effects through the free-surface boundary condition. The agreement among these three predictions is very good. Note that all parameter values used in the analytical solution and the boundary element method (BEM) simulation are the same as those prescribed in the direct (SUTRA) numerical simulation, including the thickness of the capillary fringe which was determined according to the modeled retention curve (Figure 7). The good agreement shown in Figure 9a indicates that the new wave equation describes the groundwater responses to the boundary oscillations. The results also suggest that the capillary-effects approximation present in the analytical solution and the BEM model adequately describe the influence of the unsaturated flow on the saturated flow in the aquifer. Different values of B (0.1 and 0.3 m) were also used, and the resulting analytical predictions were found to differ noticeably from the numerical predictions (dashed and dotted-dashed curves in Figure 9a). This indicates that the wave damping is sensitive to the thickness of the capillary fringe at high frequencies. In calculating the analytical solution, we used up to 200 wave modes, which was found to be sufficient numerically. For all the modes the imaginary part of the wave number is approximately zero; that is, there is no phase shift since $n\omega d/K = 1731$ is large.

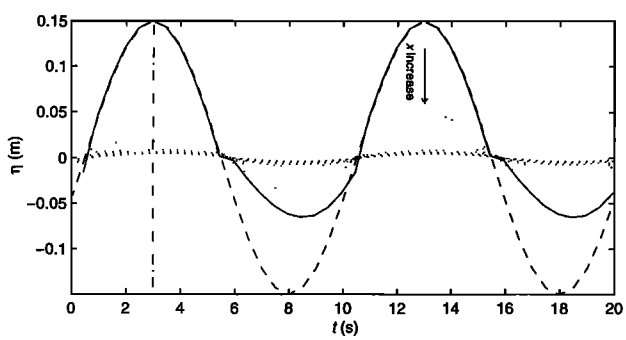

Figure 8. High-frequency water table fluctuations from Sim1. Dashed curve shows the sea level oscillations, and the solid curve is the elevations of the exit points of the water table. A seepage face was formed during the falling phase of the oscillations. Dotted curves are the elevations at various locations. The arrow indicates that as x increases, the water table fluctuation decays.

We also compare the results of the pressure oscillations, and the present analytical solution again is found to agree well with the SUTRA simulations (Figure 10). In contrast, the solution of *Nielsen et al.* [1997] failed to describe the numerical results; particularly, it predicted no oscillations at the water table, contradicting the direct numerical simulations.

To further examine the capillary effects, we explored the numerical predictions of the pressure at various locations around the water table. In analyzing the high-frequency water table fluctuations, *Li et al.* [1997] assumed that the pressure profile within the capillary fringe is linear and that the pressure at the top boundary of the capillary fringe remains constant. In Figure 11 the simulated pressure profiles above the water table (within the capillary fringe) are displayed at high and middle oceanic oscillation stages (right plot). The pressure at the top boundary of the capillary fringe (i.e., $z = 3.19$ m) is found to be approximately constant. In the unsaturated zone (above the capillary fringe), pressure changes are due to water content changes. The latter will not occur on the timescale of the period of high-frequency oceanic oscillations because the water movement in the unsaturated zone is a slow process. The simulation results also show that the pressure profile within the capillary fringe is nearly linear and that its slope varies with time, consistent with experimental data and previous modeling efforts [e.g., *Bond and Collis-George*, 1981; *Barry et al.*, 1993]. The changes of the vertical pressure gradient with a constant pressure at the top of the capillary fringe lead to oscillations of the phreatic surface, that is, water table fluctuations. These phenomena are essentially due to the capillary effects on the aquifer as described by (8) and are consistent with the analysis by *Li et al.* [1997]. To recap this analysis, we illustrate the meaning of the second term on the right-hand side of (8) in Figure 12: The vertical velocity (w) at the water table represents the pressure gradient of the linear pressure profile within the capillary fringe (s_p). As w changes with the time, the gradient of the pressure profile fluctuates. The change of pres-

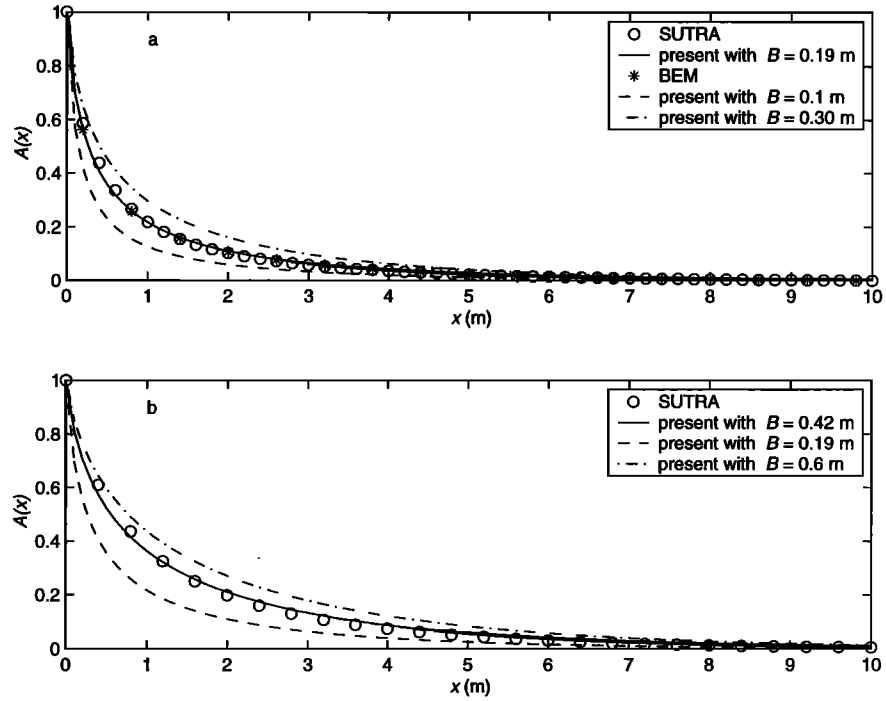

Figure 9. Comparison of the wave damping predicted by the direct numerical simulation, the present analytical solution, and the boundary element method (BEM) model of *Li et al.* [1997]: (a) Sim1 and $B = 0.19$ m and (b) Sim2 and $B = 0.42$ m.

sure gradient (Δs_p), proportional to the change of w, leads to the water table fluctuations ($\Delta\eta$) since the pressure at the top boundary of the capillary fringe is a constant. The pressure within the capillary fringe can change quickly because the water saturation in the fringe is close to unity (Figure 7). Therefore high-frequency water table fluctuations are essentially pressure responses to the oceanic oscillations.

Another simulation was conducted with a different type of

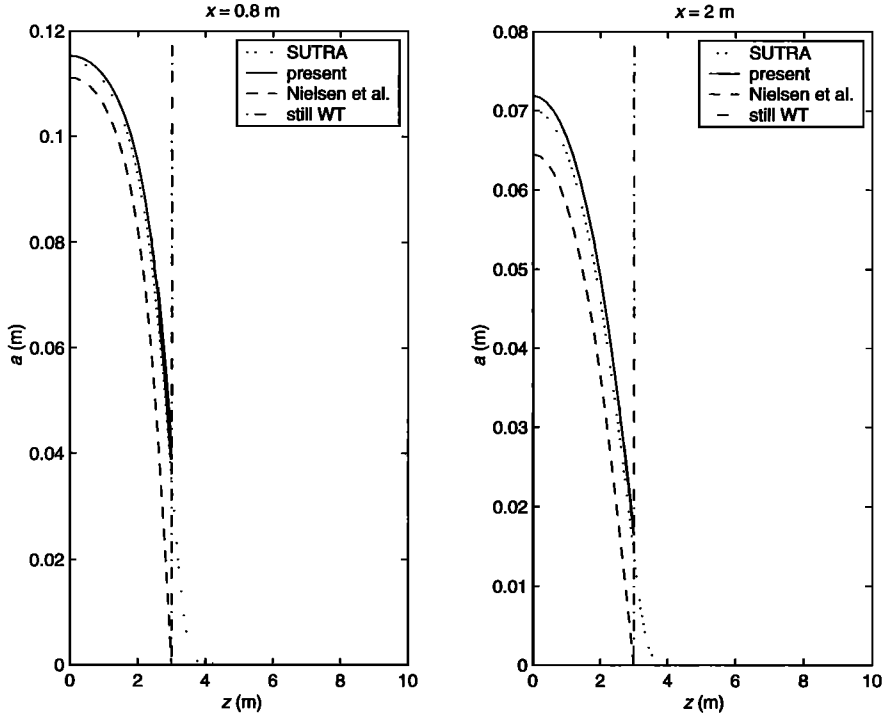

Figure 10. Comparison of the amplitude of the pressure oscillations predicted by the direct numerical simulation, the present analytical solution, and the solution of *Nielsen et al.* [1997].

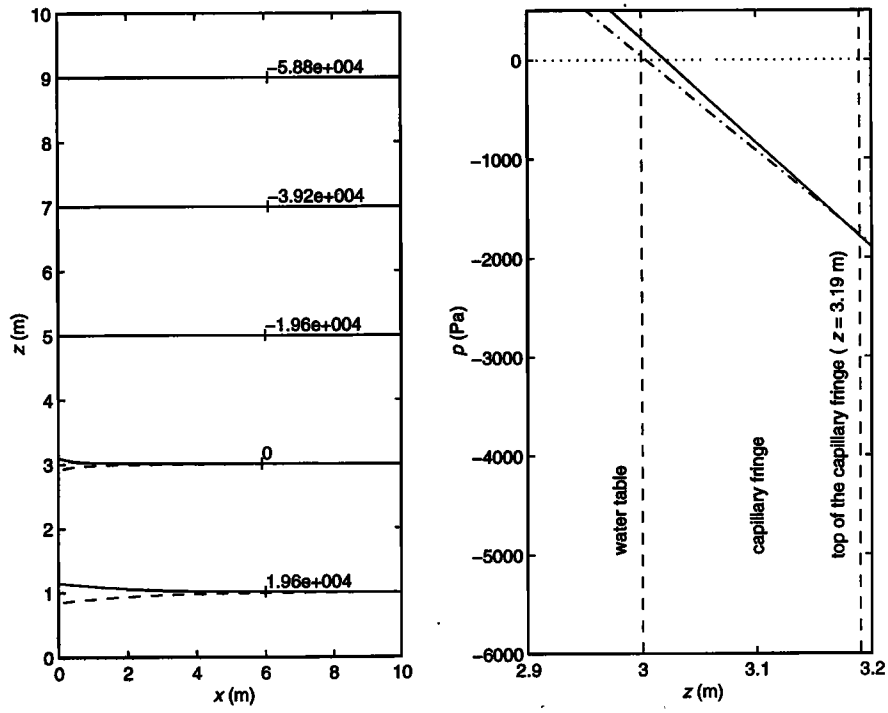

Figure 11. (left) Pressure (in pascals) contours at high (solid curve) and low oscillation (dashed curve) stages from SUTRA simulations. (right) Simulated pressure profiles within the capillary fringe from SUTRA. Solid curve is for the high oscillation stage, and dotted-dashed curve is for the mid oscillation stage.

retention characteristic for the unsaturated zone as shown by the dashed curve in Figure 7a, in which case B equals 0.42 m. Again, the analytical solution is found to describe wave damping predicted by the direct numerical simulation, and the results are sensitive to the estimate of B (Figure 9b).

3.2. Effects of Aquifer Depth

The inclusion of capillary effects in the new groundwater wave equation prevents the analytical solution from becoming nonphysical at high frequencies. However, as the aquifer depth increases, the wave number will still approach $[(2j - 1)\pi]/2d$, leading, again, to nonphysical solutions. However, the limiting process (i.e., taking d to infinity) violates the premise used in the derivation of the wave equation, which was based on the Rayleigh expansion of the potential function in terms of the vertical elevation (z). Thus the aquifer depth needs to be finite for the expansion to be valid. It is therefore expected that the solution will not apply in the limit of a very deep aquifer. However, the solution based on the intermediate-depth groundwater wave equation should collapse to the one predicted by the modified Boussinesq equation [*Barry et al.*, 1996] when a shallow aquifer is considered. Taking the limit of (1) and (7) with d going to zero shows this.

To examine the effects of the aquifer depth, we conducted another two simulations with small and large aquifer depths. In both simulations we considered high-frequency oceanic oscillations. Figure 13a compares the predicted amplitude damping in a shallow aquifer. The present analytical solution agrees well with the SUTRA simulation results. The analytical solution of *Barry et al.* [1996] based on the modified Boussinesq equation is also found to perform well. Both analytical solutions, in fact,

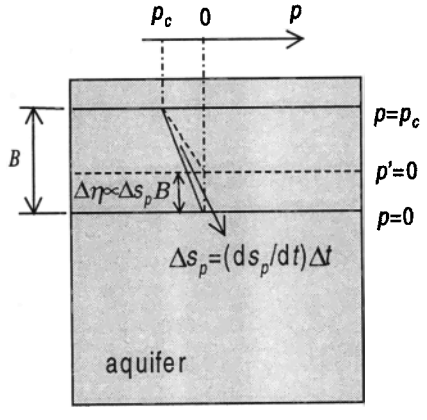

Free-surface boundary condition:

$$n\frac{\partial \eta}{\partial t} = w(x,d,t) + \frac{B}{K}\frac{\partial w(x,d,t)}{\partial t}$$

Vertical pressure gradient in capillary fringe:

$$s_p = \frac{dp}{dz} \propto \left[-\frac{1}{K}w(x,d,t) - 1\right]$$

Figure 12. Schematic diagram of capillary effects on the water table fluctuations.

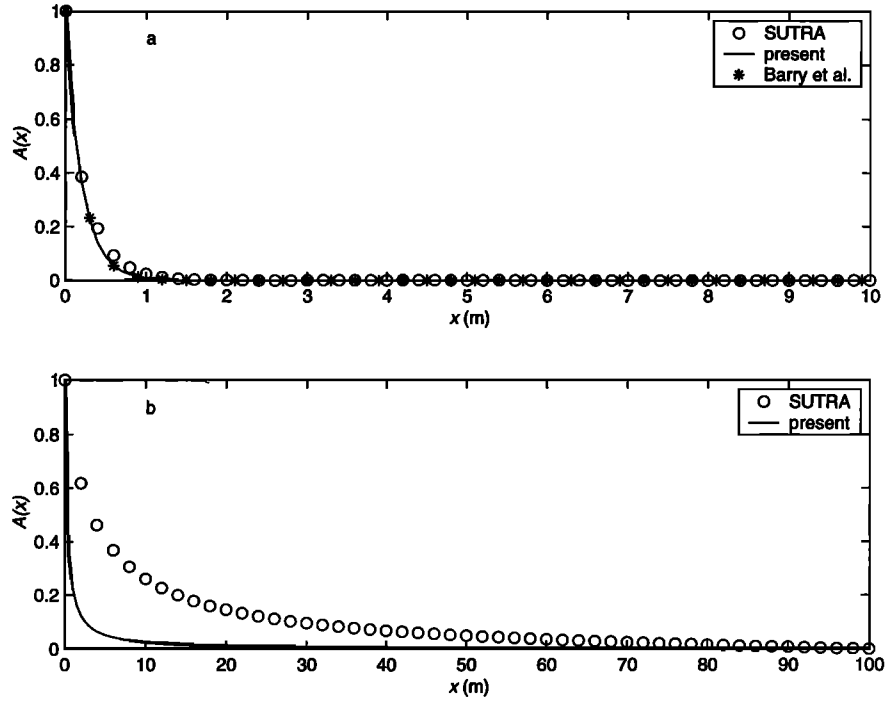

Figure 13. (a) Comparison of the wave damping predicted by the direct numerical simulation (Sim3), the present analytical solution, and that of *Barry et al.* [1996] for a shallow aquifer. (b) Comparison of the wave damping predicted by the direct numerical simulation (Sim4) and the present analytical solution for a deep aquifer.

overlap with each other. At high frequencies the solution of *Barry et al.* [1996] predicts a simple form for the amplitude decay: $A(x) = \exp[-(\sqrt{n/Bd})x]$. The results of a deep aquifer are shown in Figure 13b. It is clear that the analytical solution fails in this case.

4. Conclusion

A new groundwater wave equation has been developed by combining the effects of capillarity and vertical flows in coastal aquifers. The new equation resolves the difficulties with the equation of *Nielsen et al.* [1997] in predicting high-frequency groundwater waves.

We have verified the new wave equation by comparing its solution of the water table fluctuations and internal pressure oscillations with those from direct numerical simulations using SUTRA. The new analytical solution was found to describe well the aquifer's responses to high-frequency boundary oscillations provided that the aquifer is of a shallow or intermediate depth. For shallow aquifers the new solution reduces to the solution of *Barry et al.* [1996], which appears as a limiting case of the present theory.

In this study a vertical interface with a uniform head fluctuation was assumed to allow an analytical solution to be obtained for the derived groundwater wave equation. With this solution the validity of the new governing equation can be examined. The equation, however, can be applied to a sloping beach with swash motion, in which case a moving boundary is involved and numerical solutions are required.

Notation

A normalized amplitude of the oscillation, a/a_0.
a amplitude of the oscillation $[L]$.
a_0 amplitude of the oscillation at the ocean-aquifer interface $[L]$.
B thickness of the capillary fringe $[L]$.
d aquifer depth $[L]$.
h oscillating pressure head $[L]$.
i $\sqrt{-1}$.
K hydraulic conductivity $[L\ T^{-1}]$.
n effective porosity.
p capillary pressure, Pa.
s water saturation.
s_p pressure gradient in the capillary fringe.
t time $[T]$.
T period of the oscillation $[T]$.
w vertical flow velocity $[L\ T^{-1}]$.
x coordinate in the cross-shore direction $[L]$.
z coordinate in the vertical direction $[L]$.
η fluctuation of the water table $[L]$.
κ wave number $[L^{-1}]$.
ω frequency of the oscillation $[T^{-1}]$.

References

Barry, A. A., J.-Y. Parlange, G. C. Sander, and M. Sivaplan, A class of exact solutions for Richards' equation, *J. Hydrol.*, *142*, 29–46, 1993.

Barry, D. A., S. J. Barry, and J.-Y. Parlange, Capillarity correction to periodic solutions of the shallow flow approximation, in *Mixing Processes in Estuaries and Coastal Seas*, *Coastal Estuarine Stud.*, vol. 50, edited by C. B. Pattiaratchi, pp. 496–510, AGU, Washington, D. C., 1996.

Bond, W. J., and N. Collis-George, Ponded infiltration into simple soil system, 1, The saturation and transition zones in the moisture content profiles, *Soil Sci.*, *131*, 202–209, 1981.

Hegge, B. J., and G. Masselink, Groundwater-table responses to wave runup: An experimental study from western Australia, *J. Coastal Res.*, *7*, 623–634, 1991.

Kang, H.-Y., A. M. Aseervatham, and P. Nielsen, Field measurement

of wave runup and the beach water table, *Res. Rep. CE148*, Dep. Civ. Eng., Univ. of Queensland, St. Lucia, Queensland, Australia, 1994.

Lanyon, J. A., I. G. Eliot, and D. J. Clarke, Groundwater-level variation during semidiurnal spring tidal cycles on a sandy beach, *Aust. J. Mar. Freshwater Res.*, *33*, 377–400, 1982.

Lewandowski, A., and R. Zeidler, Beach groundwater oscillations, paper presented at 16th International Conference on Coastal Engineering, Am. Soc. of Civ. Eng., Hamburg, Germany, 1978.

Li, L., D. A. Barry, J.-Y. Parlange, and C. B. Pattiaratchi, Beach water table fluctuations due to wave runup: Capillarity effects, *Water Resour. Res.*, *33*, 935–945, 1997.

Li, L., D. A. Barry, F. Stagnitti, and J.-Y. Parlange, Tidal along-shore groundwater flow in a coastal aquifer, *Environ. Model. Assess.*, *4*, 179–188, 1999a.

Li, L., D. A. Barry, J.-Y. Parlange, and C. B. Pattiaratchi, Reply to comments by P. Nielsen on "Beach water table fluctuations due to wave runup: Capillarity effects" by Li et al., *Water Resour. Res.*, *35*, 1325–1327, 1999b.

Nielsen, P., Tidal dynamics of the water table in beaches, *Water Resour. Res.*, *26*, 2127–2135, 1990.

Nielsen, P., J. D. Fenton, R. A. Aseervatham, and P. Perrochet, Watertable waves in aquifers of intermediate depths, *Adv. Water Resour.*, *20*, 37–43, 1997.

Parlange, J.-Y., and W. Brutsaert, A capillary correction for free surface flow of groundwater, *Water Resour. Res.*, *23*, 805–808, 1987.

Turner, I. L., and P. Nielsen, Rapid water table fluctuations within the beach face: Implications for swash zone sediment transport, *Coastal Eng.*, *32*, 45–59, 1997.

van Genuchten, M. T., A closed-form equation for predicting the hydraulic conductivity of unsaturated soils, *Soil Sci. Soc. Am. J.*, *48*, 703–708, 1980.

Voss, C. I., A finite-element simulation model for saturated-unsaturated, fluid-density-dependent ground-water flow with energy transport or chemically-reactive single-species solute transport, *U.S. Geol. Surv. Water Resour. Invest. Rep.*, *84-4369*, 409 pp., 1984.

Waddell, E., Swash-groundwater-beach profile interactions, *Spec. Publ. Soc. Econ. Paleontol. Mineral.*, *24*, 115–125, 1976.

D. A. Barry and L. Li, School of Civil and Environmental Engineering and Contaminated Land Assessment and Remediation Research Centre, University of Edinburgh, The King's Buildings, Edinburgh EH9 3JN Scotland, UK. (A.Barry@ed.ac.uk; ling.li@ed.ac.uk)

J.-Y. Parlange, Department of Agricultural and Biological Engineering, Cornell University, Ithaca, NY 18453-5701. (jp58@cornell.edu)

F. Stagnitti, School of Ecology and Environment, Deakin University, Warrnambool, Victoria 3280, Australia. (frankst@deakin.edu.au)

(Received July 12, 1999; revised September 22, 1999; accepted October 14, 1999.)